

## Supporting Information

### **[V@Ge<sub>8</sub>As<sub>4</sub>]<sup>3-</sup> and [Nb@Ge<sub>8</sub>As<sub>6</sub>]<sup>3-</sup>: Encapsulation of Electron-Poor Transition Metal Atoms**

Stefan Mitzinger,<sup>a</sup> Lies Broeckaert,<sup>a,b</sup> Werner Massa,<sup>a</sup> Florian Weigend,<sup>b\*</sup> and Stefanie Dehnen<sup>a\*</sup>

<sup>a</sup> *Fachbereich Chemie, Wissenschaftliches Zentrum für Materialwissenschaften, Philipps-Universität Marburg, Hans-Meerwein-Straße, 35043 Marburg, Germany, email: dehnen@chemie.uni-marburg.de;*

<sup>b</sup> *Institut für Nanotechnologie, Karlsruher Institut für Technologie (KIT) Hermann-von-Helmholtz-Platz 1, 76344 Eggenstein-Leopoldshafen, Germany, email: florian.weigend@kit.edu*

#### **Contents:**

1. *Synthesis details*
2. *X-ray crystallography*
3. *Energy dispersive X-ray spectroscopy (EDX)*
4. *Electrospray Ionization Mass Spectrometry (ESI-MS) Investigations*
5. *Quantum Chemical Investigations*
6. *References for the Supporting Information*

## 1. Synthesis details

### 1.1 General

All manipulations and reactions were performed under dry Ar atmosphere by using standard Schlenk or glovebox techniques. All solvents were dried and freshly distilled prior to use. [2.2.2]crypt<sup>[1a]</sup> (Merck) was dried *in vacuo* for at least 18 h.

A phase with a nominal composition “KGeAs” was addressed by combining K, Ge and As in equimolar amounts in a niobium ampoule. The ampoule was then sealed by arc-welding and was placed in an oven at 950 °C. The resulting solid contained some single crystals of the known phase.<sup>[1b]</sup> It was ground in a mortar and analysed by means of powder X-ray diffractometry and energy dispersive X-ray (EDX) spectroscopy. The powder diffraction pattern confirmed the existence of K<sub>2</sub>GeAs<sub>2</sub>. Additional reflections could not be explained with any phase known in the ICSD database for any combination of the given elements (see 2.3). To our surprise, the EDX analysis revealed the presence of Nb with 3.1 atom-% within the resulting product. This accords with an overall stoichiometry near to “K<sub>10</sub>Ge<sub>10</sub>As<sub>10</sub>Nb”, thus close to the Ge:As:Nb ratio found in the [Nb@Ge<sub>8</sub>As<sub>6</sub>]<sup>3-</sup> anion (see below). The other elements appeared in near to equimolar ratios, as expected. In the related work by *von Schnering* and co-workers, the compound containing the [NbAs<sub>8</sub>]<sup>3-</sup> anion was reproduced by directed synthesis with Nb<sub>2</sub>O<sub>5</sub>.<sup>[1c]</sup> This indicated the possibility of an Nb<sub>2</sub>O<sub>5</sub> impurity to take place in the fusion reaction. We cannot exclude a contribution of such an impurity to the generation of the starting material in our case, but we suppose that the purity of the tube material (≥99.8%) does not allow for an impurity that results in a 3.1 atomic-% in the starting material. The powder diffraction pattern does not indicate the presence of (crystalline) Nb<sub>2</sub>O<sub>5</sub> (see 2.3). We did not use Nb<sub>2</sub>O<sub>5</sub> directly, as we have always strictly excluded oxygen from our reactions so far.

Upon the synthesis of the Nb compound (see below), we attempted to generate a homologue V compound. For this, the phase “K<sub>8</sub>Ge<sub>8</sub>As<sub>6</sub>V” was approached by fusing K, Ge, As and V in an 8:8:6:1 stoichiometric ratio – thereby adopting the As amount to the stoichiometric ratio observed in the [Nb@Ge<sub>8</sub>As<sub>6</sub>]<sup>3-</sup> anion – in a silica glass ampoule with an oxygen torch. *Caution: heating of K in silica glass ampoules needs to be carried out with care!* The resulting solid was thoroughly ground in a mortar prior to further use. In the X-ray powder diagram (see 2.3), K<sub>2</sub>GeAs<sub>2</sub> could be identified, and elemental Ge. EDX analysis confirmed the presence of V with 3.0 atom-% in the intermetallic phase, indicating a smaller amount to be included in the intermetallic phase than attempted. We assume a side reaction of V with the silica tube material

(yielding  $V_2O_5$ , for instance) to be responsible for the small loss of V during the fusion reaction. However, the fusion product does not contain (crystalline)  $V_2O_5$  as indicated in the powder diagram (see 2.3). The other elements appeared in the expected ratios.

## 1.2 Syntheses

### 1.2.1 Synthesis of $[K([2.2.2]crypt)_3[V@Ge_8As_4] \cdot 2tol \cdot en$ (1)

139 mg (0.1 mmol) of the K/Ge/As/V intermetallic solid and 139 mg of [2.2.2]crypt were weighed out into a Schlenk tube. Then *en* (ethane-1,2-diamine, 4 mL) was added. The reaction mixture was allowed to stir for 2 days. The liquid was filtered through a standard glass frit, yielding a orange solution that was carefully layered by *tol* (toluene, 7 mL). After 21 days, yellow plate shaped crystals of  $[K([2.2.2]crypt)_3[V@Ge_8As_4] \cdot 2tol \cdot en$  (1) were obtained in approximately 12% yield.

### 1.2.2 Synthesis of $[K([2.2.2]crypt)_3[Nb@Ge_8As_6] \cdot tol \cdot en$ (2)

187 mg (1 mmol) of the K/Ge/As/Nb intermetallic solid and 141 mg [2.2.2]crypt (0.375 mmol) were weighed out into a Schlenk tube. Then *en* (ethane-1,2-diamine, 4 mL) was added. The reaction mixture was allowed to stir for 2 days. The liquid was filtered through a standard glass frit, yielding a dark red solution that was carefully layered by *tol* (toluene, 7 mL). After 7 days dark red block shaped crystals of  $[K([2.2.2]crypt)_3[Nb@Ge_8As_6] \cdot tol \cdot en$  (2) were obtained in approximately 22% yield.

## 2. X-ray crystallography

Powder X-ray data of the crude phases, as used for the extraction and cluster formation step by means of *en*/[2.2.2]crypt, were collected by Ekrem Güneş (Justus-Liebig Universität, Gießen) on a Stoe StadiP powder diffractometer (Stoe, Darmstadt, Germany) using  $CuK\alpha$  radiation, and were evaluated with the X'Pert Highscore Plus software.<sup>[2a]</sup>

The data for the single-crystal X-ray structural analyses were collected at  $T = 100(2)$  K with  $Mo-K\alpha$ -radiation ( $\lambda_{Mo-K\alpha} = 0.71073$  Å) on an area detector system Stoe IPDS2. The structures were solved by direct methods (SHELXS-97<sup>[2b]</sup>), and refined by full-matrix-least-squares methods against  $F^2$  with program SHELXL-2013.<sup>[2b]</sup> Crystallographic data for the two structures reported in this paper have been deposited with the Cambridge Crystallographic Data Center as supplementary publications nos. CCDC-1030791 (1) and CCDC-1030792 (2). The crystal data and experimental parameters of the structure determinations are collected in Table S1.

**Table S1.** Crystal data and details of the structure determinations of **1** and **2**.

Compound	1	2
empirical formula	C <sub>70</sub> H <sub>132</sub> As <sub>4</sub> Ge <sub>8</sub> K <sub>3</sub> N <sub>8</sub> O <sub>18</sub> V	C <sub>63</sub> H <sub>124</sub> As <sub>6</sub> Ge <sub>8</sub> K <sub>3</sub> N <sub>8</sub> NbO <sub>18</sub>
formula weight [g mol <sup>-1</sup> ]	2422.47	2522.14
crystal color, shape	block, red	block, red
crystal size [mm <sup>3</sup> ]	0.48 × 0.31 × 0.20	0.50 × 0.50 × 0.40
crystal system	triclinic	triclinic
space group	P $\bar{1}$	P $\bar{1}$
a [Å]	11.9985(7)	16.1475(7)
b [Å]	16.7415(11)	16.7769(6)
c [Å]	25.3291(18)	18.0373(8)
$\alpha$ [°]	80.709(6)	89.184(3)
$\beta$ [°]	88.755(5)	80.452(3)
$\gamma$ [°]	69.258(5)	79.420(3)
V [Å <sup>3</sup> ]	4692.3(6)	4736.1(3)
Z, $\rho_{\text{calc}}$ [g cm <sup>-3</sup> ]	2, 1.715	2, 1.769
$\mu$ (MoK $\alpha$ ) [mm <sup>-1</sup> ]	4.215	4.889
absorption correction type	numerical	numerical
2 $\theta$ range [°]	2.55-25.00	3.01-26.00
total reflns	41618	66699
unique reflns [ $R_{\text{int}}$ ]	16426 [0.109]	18581 [0.080]
obs. reflns [ $I > 2\sigma(I)$ ]	4761	8558
parameters	886	945
$wR_2$ (all data)/ $R_1$ [ $I > 2\sigma(I)$ ]	0.1194/0.0598	0.0628/0.0346
Goof (all data)	0.687	0.633
max peak/hole, [e Å <sup>-3</sup> ]	0.972/-0.738	1.084/-0.507

### 2.1 Details of the structure determination of [K([2.2.2]crypt)<sub>3</sub>[V@Ge<sub>8</sub>As<sub>4</sub>]-2tol-en (1)

A numerical absorption correction (Gaussian integration) has been applied based on crystal faces optimized by the XSHAPE procedure in XAREA (Stoe 2013).

**Cluster anion:** The main component is a V-centered 12-atom cluster with the composition [V@Ge<sub>8</sub>As<sub>4</sub>]<sup>3-</sup> according to theoretical calculations (see section 5). After refinement of this cluster anion, five residual electron density maxima were observed and could be refined as Ge/As atoms with occupations up to 13%. *Vice versa*, underoccupations of up to 13% were observed for several of the 12 main cluster atoms. This feature can be explained by assuming disorder over two additional orientations. The atom positions for the latter were obtained by fitting the geometry of the main component to five atom or peak positions that belonged clearly to the respective orientation. Refinement of a respective disorder model gave occupations for the three orientations of 82.6(1), 9.0(1), and 8.4(1)%, respectively. The critical refinement of many close metal positions was stabilized by applying geometrical

restraints favoring the same geometry for all three cluster shells (SAME option in SHELXL). Atoms with neighbors closer than 1 Å were refined with the same anisotropic displacement parameters. In the final cycles, all metal positions were refined with the expected overall ratio Ge/As 8:4. As Ge and As have virtually the same scattering power with Mo radiation, errors in the assignment would not influence the quality of the refinement. The correctness of this model is documented in good convergence of the refinement and the fact that for all atoms reasonable anisotropic displacement parameters could be refined. In Figure 1 of the main document, only the main component of the anion is shown with Ge/As attributions according to the perturbation theoretical calculations (see section 5). In Figure S1, the complete disorder model is shown with the labelling scheme. Bond lengths are given in Table S2.

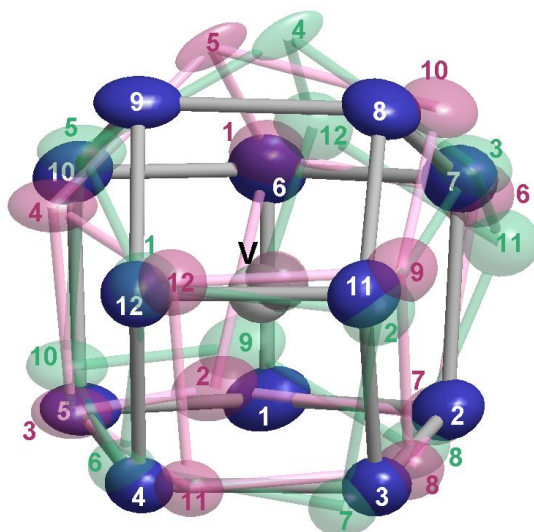


**Figure S1.**  $[V@Ge_8As_4]^{3-}$  anion in **1** disordered over three orientations (blue 82.6%, red 9.0%, green 8.4%). Displacement ellipsoids at the 50% probability level.

**Table S2.** Interatomic distances [Å] in the anion of **1** [I: main orientation (82.6%), II: 2<sup>nd</sup> (9.0%), III: 3<sup>rd</sup> orientation (8.4%)].

	atom numbers		atom numbers		atom numbers	
I II III	1 – 2	2.531(3) 2.62(2) 2.57(2)	3 – 11	2.522(3) 2.44(1) 2.43(1)	7 – 8	2.489(3) 2.47(2) 2.46(2)
I II III	1 – 5	2.464(3) 2.48(2) 2.47(2)	4 – 5	2.474(3) 2.62(1) 2.63(1)	8 – 9	2.655(3) 2.61(2) 2.57(2)
I II III	1 – 6	2.514(3) 2.51(2) 2.50(2)	4 – 12	2.515(3) 2.49(2) 2.46(1)	9 – 10	2.487(2) 2.47(2) 2.46(2)
I II III	2 – 3	2.470(5) 2.33(1) 2.36(2)	5 – 10	2.580(2) 2.77(1) 2.86(1)	9 – 12	2.515(3) 2.51(2) 2.56(2)
I II III	2 – 7	2.529(3) 2.57(2) 2.54(2)	6 – 7	2.478(3) 2.45(2) 2.45(2)	11 – 12	2.493(3) 2.56(2) 2.56(2)
I II III	3 – 4	2.595(3) 2.54(1) 2.63(1)	6 – 10	2.436(3) 2.36(2) 2.35(2)	average	<b>2.515</b> <b>2.518</b> <b>2.521</b>
I II III	V – 1	2.841(3) 2.81(1) 2.82(2)	V – 5	2.624(3) 2.67(1) 2.62(1)	V – 9	2.678(3) 2.69(2) 2.70(2)
I II III	V – 2	2.621(3) 2.65(1) 2.65(2)	V – 6	2.771(3) 2.78(2) 2.79(2)	V – 10	2.714(3) 2.68(1) 2.67(1)
I II III	V – 3	2.730(3) 2.72(1) 2.68(1)	V – 7	2.747(3) 2.74(2) 2.76(2)	V – 11	2.804(3) 2.80(1) 2.80(1)
I II III	V – 4	2.674(3) 2.64(1) 2.70(1)	V – 8	2.653(3) 2.67(2) 2.76(2)	V – 12	2.786(3) 2.78(1) 2.78(1)
I II III					average	<b>2.720</b> <b>2.719</b> <b>2.728</b>

**Cations:** Two of three [K([2.2.2]crypt)]<sup>+</sup> cations are well localized. A third one shows disorder over two positions shifted by about 1 Å. For it only isotropic displacement parameters could be refined common by pairs. All cations were refined using geometrical restraints on the bond lengths and 1,3-distances but leaving conformational freedom (SAME option of SHELXL). This explains the large number of restraints. Figure S2 shows all three cations.

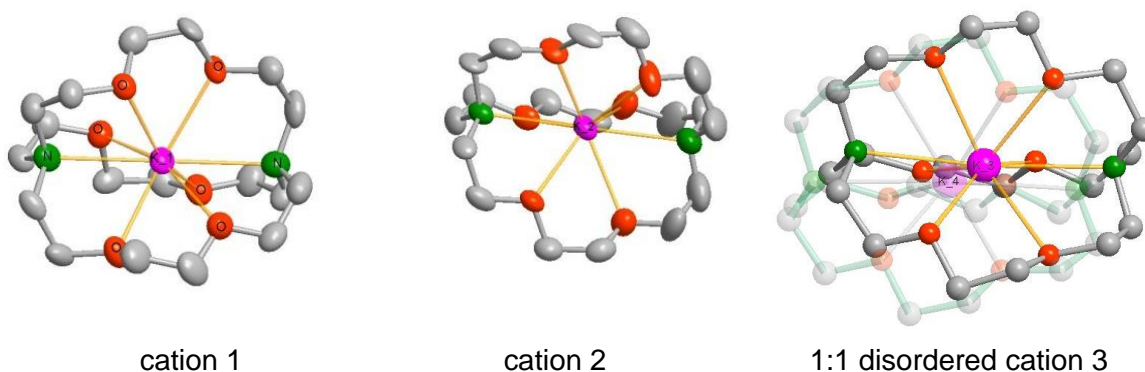


**Figure S2.** The three independent  $[K([2.2.2]crypt)]^+$  cations in **1**. Displacement ellipsoids for cations 1 and 2 at the 50% probability level, for 3 arbitrary radii.

**Solvent:** Around the unit cell origin, a large void remained with diffuse electron densities corresponding to about 140 electrons/asymm. unit. Thus, similar to the structure of **2**, solvent contents of toluene and *en* molecules are assumed, probably two toluene and one *en* molecules according to the electron count. As we were not able to establish a sensible disorder model for this region, its contribution was subtracted by back Fourier transform (PLATON SQUEEZE) from the data set. Thus, the solvent molecules are missing in the parameter list leading to several error messages in the PLATON CHECKCIF procedure.

**Packing:** The three independent cations form layers parallel to the (0-11) plane. In between, the anion clusters are inserted (Figure S3), as well as the disordered solvent molecules.

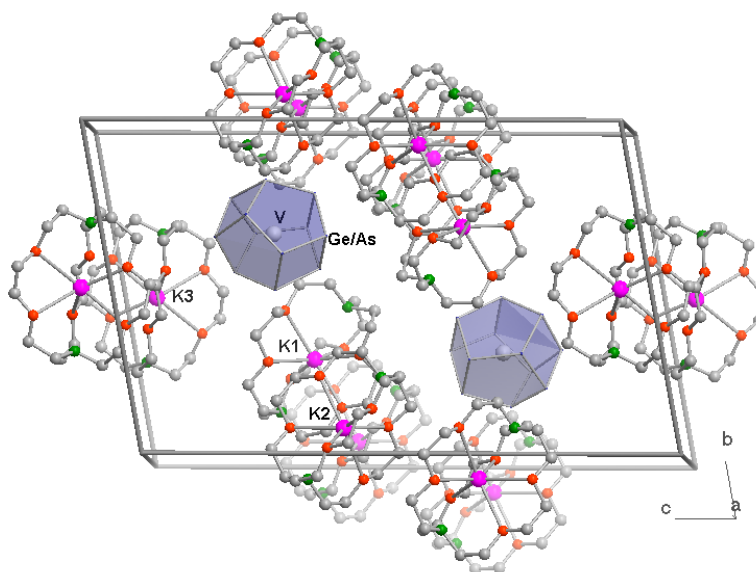


**Figure S3.** Unit cell of **1** with neighborhood. Arbitrary radii; polyhedra: anionic clusters (main orientation), pink: K, green: N, red: O, grey: C. Note that the empty space around the cell origin contains non-localized, disordered toluene and *en* solvent molecules.

## 2.2 Details of the structure determination of $[K([2.2.2]crypt)_3[Nb@Ge_8As_6] \cdot tol \cdot en (2)$

As for **1**, a numerical absorption correction has been applied based on crystal faces optimized by the XSHAPE procedure in XAREA (Stoe 2013).

The anion revealed as a pure  $[Nb@Ge_8As_6]^{3-}$  cluster. The Ge/As assignment (Figure 1 and Figure S4) was done based on the perturbation theoretical calculations (section 5). The interatomic distances are collected in Table S3. The three independent  $[K([2.2.2]crypt)]^+$  cations are all well localized (Figure S5). Even the solvent content, a toluene and an *en* molecule, could be localized and refined. Only the *en* molecule had to be refined with restraints of the bond lengths and with isotropic displacement parameters.

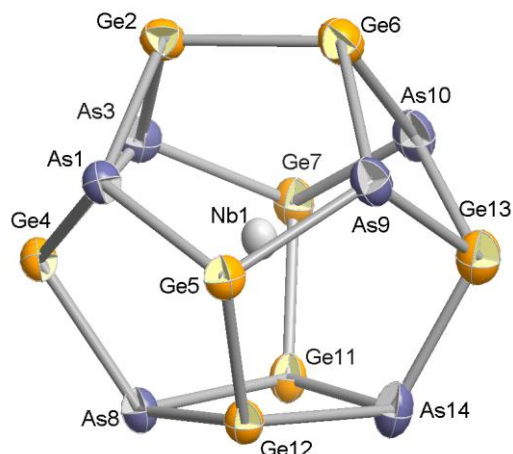


**Figure S4.**  $[Nb@Ge_8As_6]^{3-}$  anion in **2**. Displacement ellipsoids at the 50% probability level.

**Table S3.** Interatomic distances [ $\text{\AA}$ ] in the anion of **2**.

atom numbers		atom numbers		atom numbers	
As1 – Ge2	2.5111(9)	Ge4 – As8	2.4817(9)	As8 – Ge11	2.4950(9)
As1 – Ge4	2.5125(9)	Ge5 – As9	2.4733(9)	As8 – Ge12	2.4949(8)
As1 – Ge5	2.4803(9)	Ge5 – Ge12	2.5050(9)	As9 – Ge13	2.5099(10)
Ge2 – As3	2.5080(9)	Ge6 – As9	2.4960(9)	As10 – Ge13	2.5215(10)
Ge2 – Ge6	2.4762(10)	Ge6 – As10	2.5009(10)	Ge11 – As14	2.5057(9)
As3 – Ge4	2.5197(9)	Ge7 – As10	2.5010(10)	Ge12 – As14	2.5006(9)
As3 – Ge7	2.4741(9)	Ge7 – Ge11	2.5221(10)	Ge13 – As14	2.4505(11)
				av. Ge – As	<b>2.4965</b>
				av. Ge – Ge	<b>2.5011</b>
Nb – As1	2.7783(8)	Nb – Ge6	2.9998(9)	Nb – Ge11	2.8487(8)
Nb – Ge2	3.0327(9)	Nb – Ge7	2.9322(8)	Nb – Ge12	2.8480(8)
Nb – As3	2.8096(8)	Nb – As8	2.9416(8)	Nb – Ge13	3.0409(9)
Nb – Ge4	3.0769(9)	Nb – As9	2.8246(8)	Nb – As14	2.9736(9)
Nb – Ge5	2.9441(8)	Nb – As10	2.8094(8)	av. Nb – Ge	<b>2.9654</b>
				av. Nb – As	<b>2.8562</b>



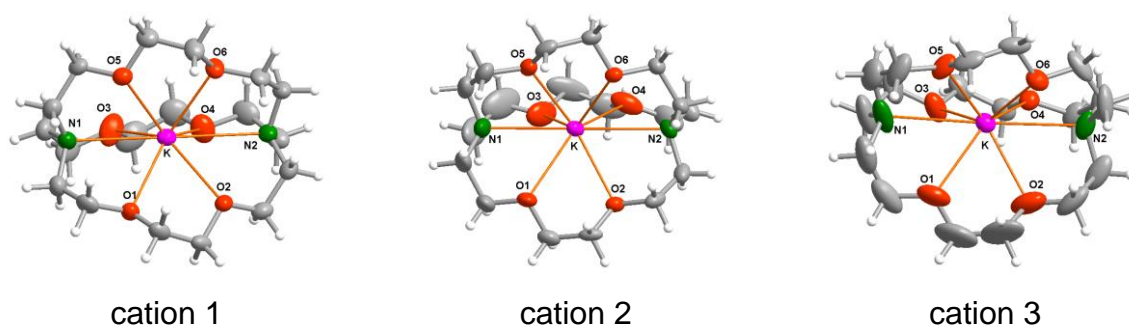


**Figure S5.** The three independent  $[K[2.2.2]crypt]^+$  cations in **2**. Displacement ellipsoids at the 50% probability level.

**Packing:** The  $[K([2.2.2]crypt)]^+$  cations form a honeycomb-like packing with channels along the  $[11-1]$  direction, in which the anion clusters are aligned (Figure S6).

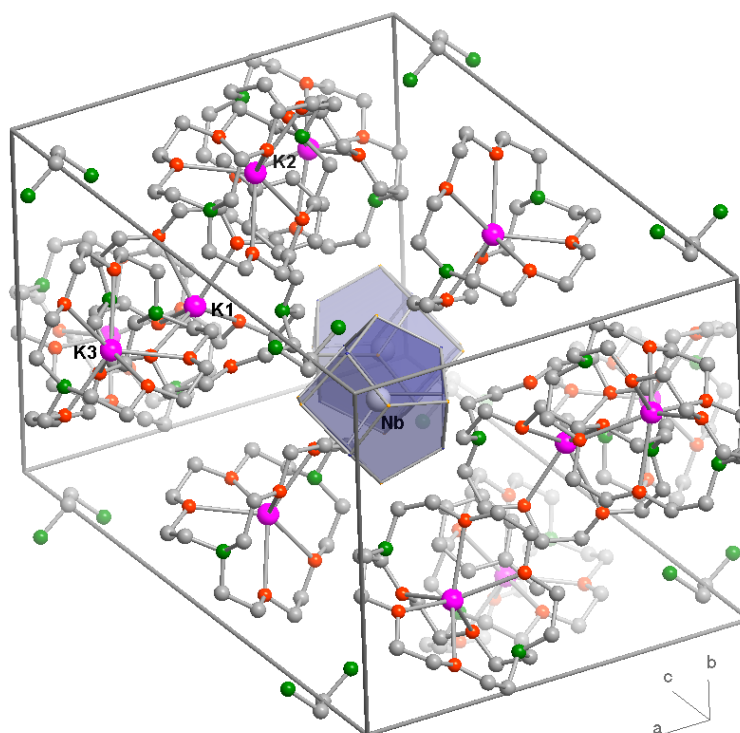


**Figure S6.** Unit cell of **1** with neighborhood. Arbitrary radii; blue polyhedra: anion clusters, pink: K, green: N, red: O, grey: C.

### **2.3 Powder X-ray diffraction data of the crude phases prior to cluster formation**

Figures S7 and S8 show the PXRD patterns of the solid products upon the fusion reaction (see Section 1.1), which were used for the extractions. They were compared with known phases in the respective systems and with possible oxides.

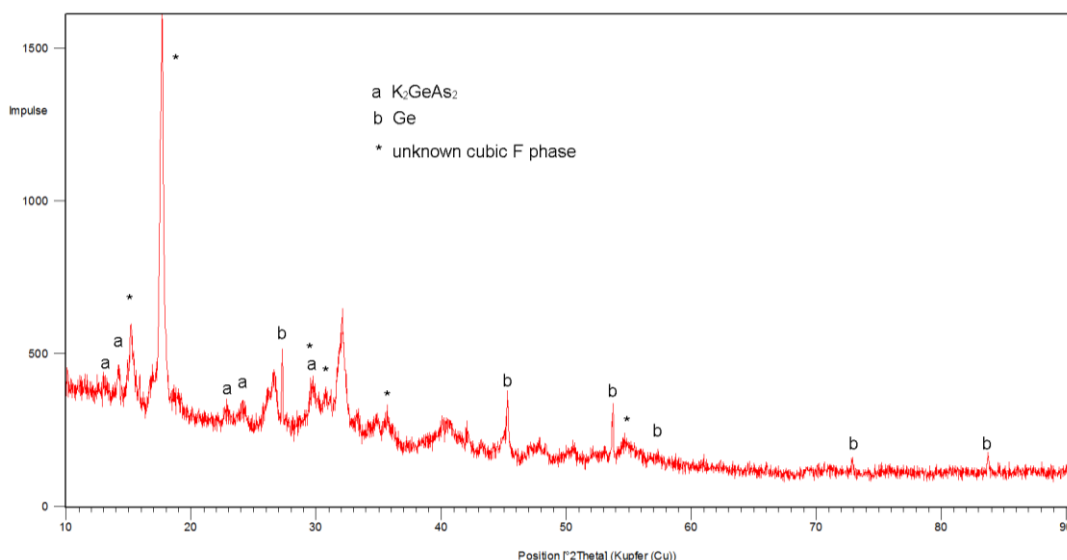


**Figure S7.** X-ray powder pattern of the K/Ge/As/V solid used for the synthesis of **1**, and possible assignments.

In the V-containing system,  $K_2GeAs_2$ <sup>[1b]</sup> could be identified as a minor component, as well as very sharp reflections of elemental Ge. The major component (marked with \*) could be indexed with a cubic F-centered cell with  $a = 10.08 \text{ \AA}$ . There is no entry in the ICSD database with these cell and the respective atom types.

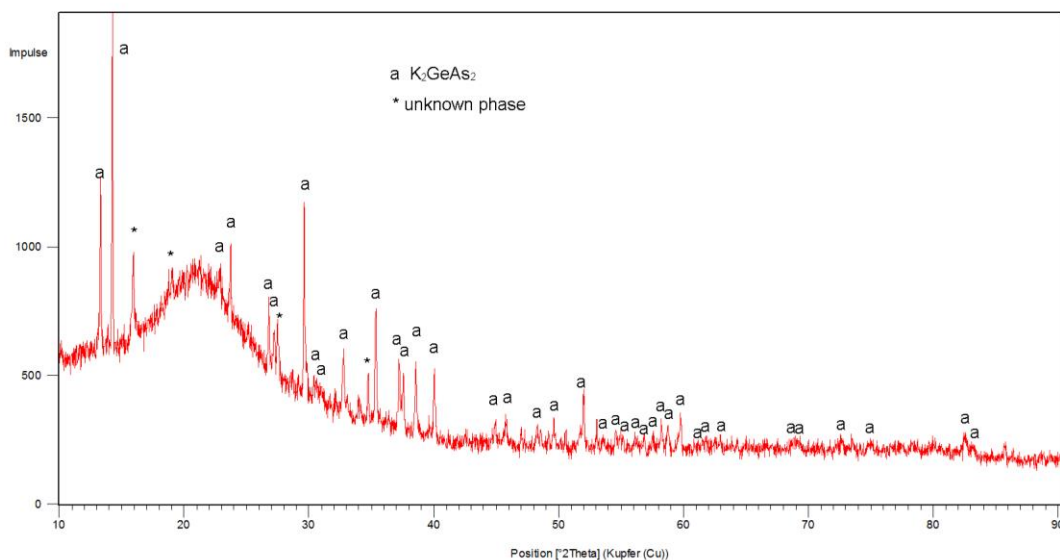


**Figure S8.** X-ray powder pattern of the K/Ge/As/Nb intermetallic solid used for synthesis and possible assignments.

The pattern of the Nb-containing solid shows a strong contribution of an amorphous phase, a large amount of  $K_2GeAs_2$ , and some additional reflections that could neither be identified nor indexed.

### 3. Energy dispersive X-ray spectroscopy (EDX) analysis

EDX analyses were performed to support the elemental composition that was suggested based on the XRD experiments. These were carried out using an EDX-device Voyager 4.0 of Noran Instruments coupled with an electron microscope CamScan CS 4DV. Data acquisition was performed with an acceleration voltage of 20 kV and 100 s accumulation time. The radiation emitted by the atoms was analyzed: K-K, Ge-K, As-K, V-K and Nb-L. To minimize surface effects in the measurement, the K-lines were preferably used to calculate the elemental composition. Results are summarized in Table S4.

**Table S4.** EDX analysis of **1** and **2** (K, Ge, As, V/Nb)

Element	k-ratio	ZAF	Atom%	Atomic ratio observed (calc)	Element wt %	wt % Err. (1-sigma)
<b>[K([2.2.2]crypt)<sub>3</sub>[Ge<sub>8</sub>As<sub>4</sub>V]·2tol·en (1)</b>						
K-K	0.1131	1.180	22.07	3.73 (3)	13.35	+/- 0.26
Ge-K	0.4835	1.033	44.47	7.23 (6)	49.95	+/- 1.77
As-K	0.3113	1.037	27.86	4.00 (4)	32.29	+/- 1.91
V-K	0.0413	1.068	5.60	0.97 (1)	4.41	+/- 0.27
Total			100	15.93 (14)	100	
<b>[K([2.2.2]crypt)<sub>3</sub>[Ge<sub>8</sub>As<sub>6</sub>Nb]·tol·en (2)</b>						
K-K	0.1174	1.226	24.43	4.77 (3)	14.40	+/- 0.21
Ge-K	0.4140	1.028	38.90	7.59 (8)	42.57	+/- 1.15
As-K	0.3363	1.032	30.74	6.00 (6)	34.72	+/- 1.37
Nb-L	0.0444	1.873	5.94	1.16 (1)	8.32	+/- 0.38
Total			100	19.52 (18)	100	

The results of the EDX investigations confirm the Ge:As ratios of the investigated substances within the expected accuracy, as well as the presence of V and Nb, respectively, in the crystalline material.

#### **4. Electrospray Ionization Mass Spectrometry (ESI-MS) Investigations**

ESI(-) mass spectrometry has been performed on a Finnigan LTQ-FT spectrometer by Thermo Fischer Scientific in the negative ion mode: Spray voltage 3.90 kV, capillary temperature 300°C, capillary voltage -11 V, tube lens voltage -140 V, sheath gas flow rate 25 arb, sweep gas flow rate 0 arb. For the measurements, the filtered solutions were dried *in vacuo* and re-dissolved in dry DMF. During the ESI-MS investigations fast decomposition was observed during the injection, resulting in black precipitate in the Hamilton syringe as well as a decreased flow rate into the ESI chamber. Additional peaks observed in the ESI(-) spectrum show incomplete isotopic patterns and are believed to belong to decomposition products and fragments formed by a dynamic re-organization of the cluster anions and their fragments in solution under ESI-MS conditions. As it is common for Zintl anions and intermetallic cluster anions, the observed fragments have been detected as oxidized, singly charged species. In summary, despite analytical challenges the existence of the cluster anions of **1** and **2** could be proven (see below).

##### **4.1 ESI-MS investigation of [K([2.2.2]crypt)]<sub>3</sub>[Ge<sub>8</sub>As<sub>4</sub>V] (**1**)**

The ESI(-)MS spectrum of **1** (Figure S9) revealed the (protonated) cluster anion [Ge<sub>8</sub>As<sub>4</sub>VH]<sup>-</sup> (m/z = 933.01) to be present along with the [K([2.2.2]crypt)]<sup>+</sup> adduct [Ge<sub>8</sub>As<sub>4</sub>VC<sub>18</sub>H<sub>37</sub>N<sub>2</sub>O<sub>6</sub>K]<sup>-</sup> (m/z = 1348.23) of the trimetallic cluster [Ge<sub>8</sub>As<sub>4</sub>V]<sup>3-</sup> found in SCXD (Figures S10, S11). Furthermore, the anions (Ge<sub>2</sub>As<sub>2</sub>H)<sup>-</sup> (m/z = 296.69), (Ge<sub>7</sub>As<sub>2</sub>)<sup>-</sup> (m/z = 658.30), (Ge<sub>7</sub>As<sub>2</sub>C<sub>18</sub>H<sub>36</sub>N<sub>2</sub>O<sub>6</sub>K)<sup>-</sup> (m/z = 1073.52), and (Ge<sub>10</sub>C<sub>18</sub>H<sub>36</sub>N<sub>2</sub>O<sub>6</sub>K)<sup>-</sup> (m/z = 1141.44) and were identified (Figures S12-S14). They are believed to origin from the formation of the multimetallic cluster itself during extraction, and they likely represent intermediates which could not be crystallized. In some spectra, unidentified components that may derive from fragmentations partially overlay the peak of the named species.

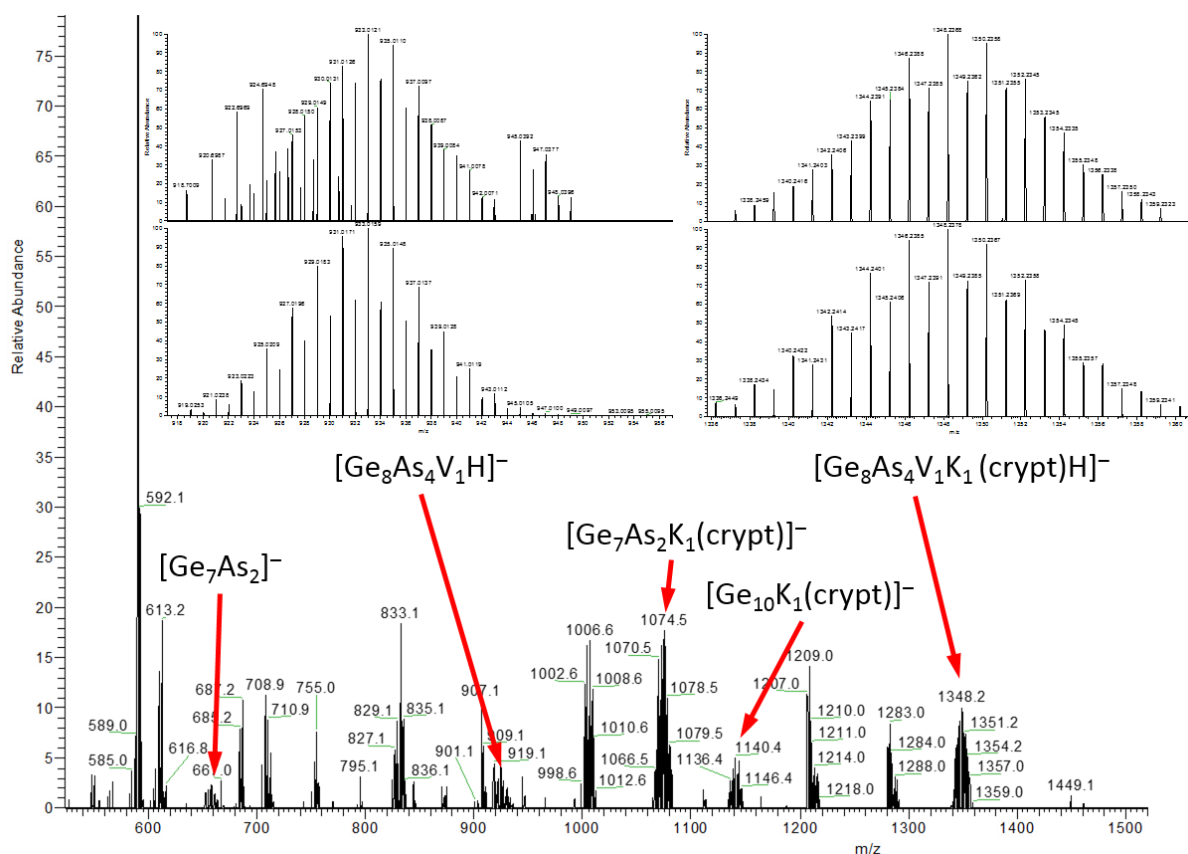


**Figure S9.** ESI-MS(-) overview spectrum

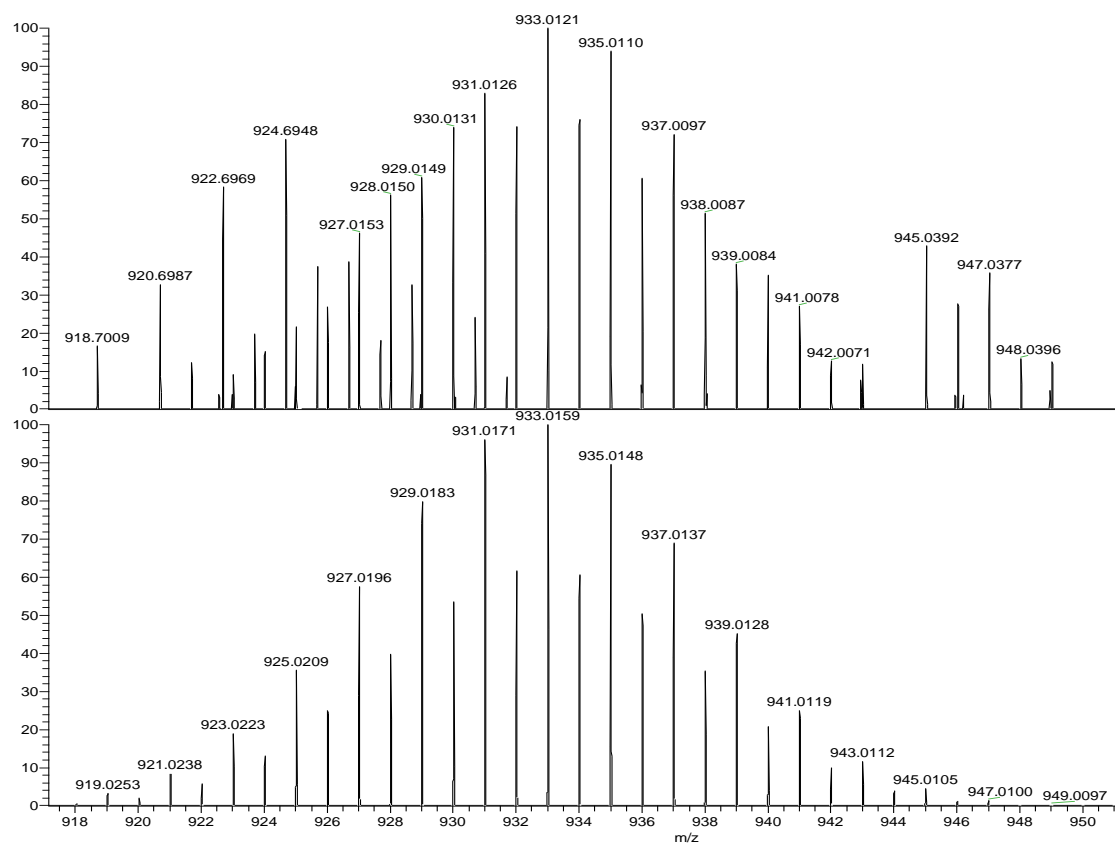


**Figure S10.** ESI-MS(-) mass peak of the  $[Ge_8As_4VH]^-$  anion. Measured (top) vs. calculated (bottom) spectrum. The partially overlaid species could not be identified.

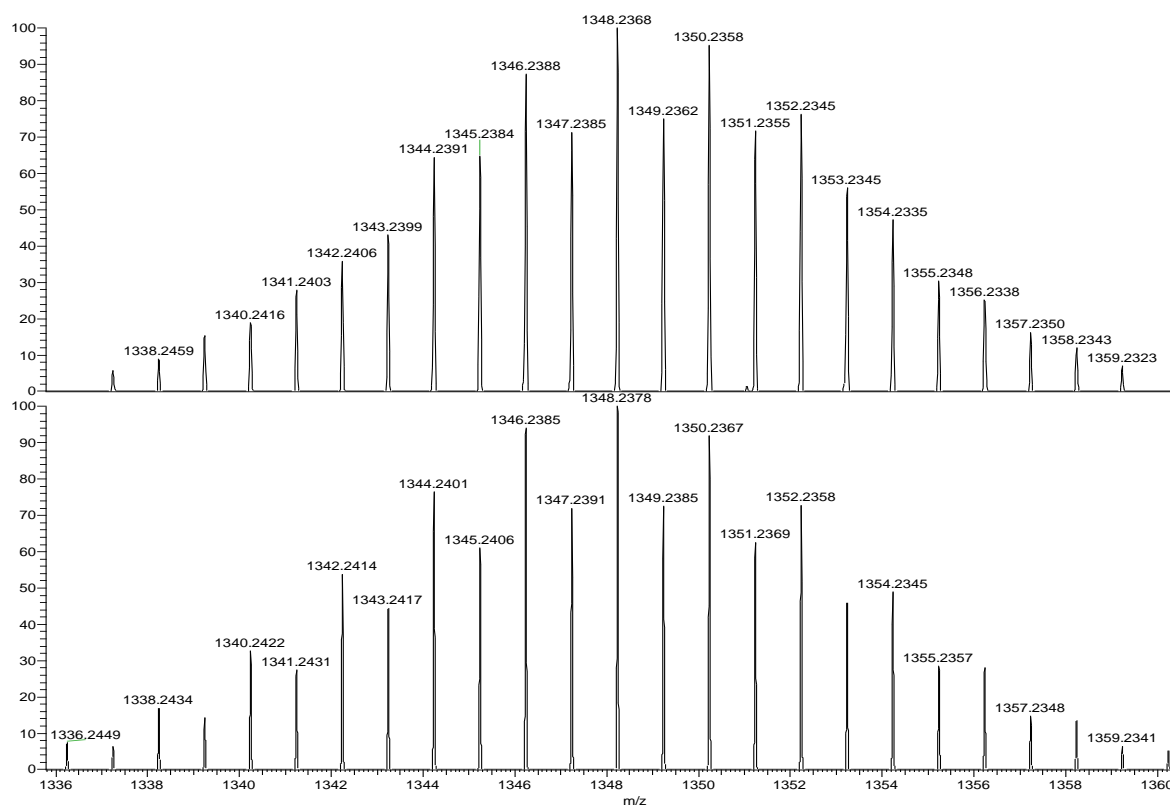


**Figure S11.** ESI(-) mass peak of  $[\text{Ge}_8\text{As}_4\text{VC}_{18}\text{H}_{37}\text{N}_2\text{O}_6\text{K}]^-$ . Measured (top) vs. calculated (bottom) spectrum.

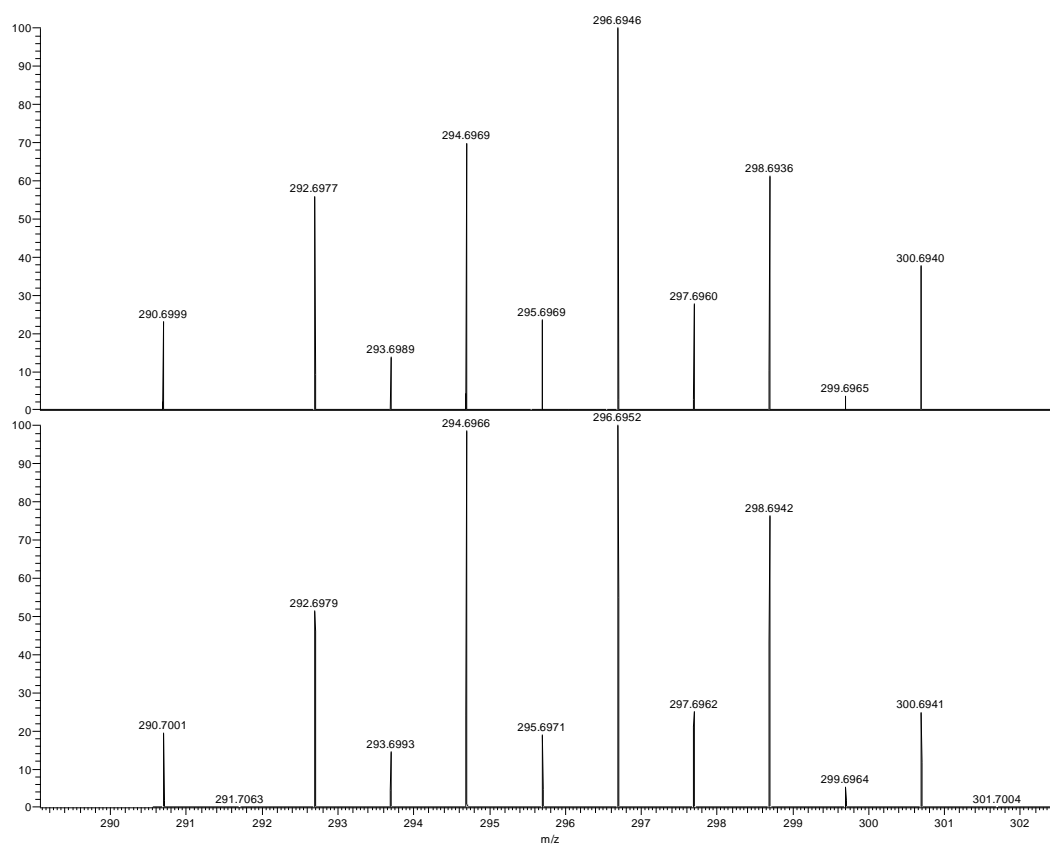


**Figure S12.** ESI(-) mass peak of  $(\text{Ge}_2\text{As}_2\text{H})^-$ . Measured (top) vs. calculated (bottom) spectrum.

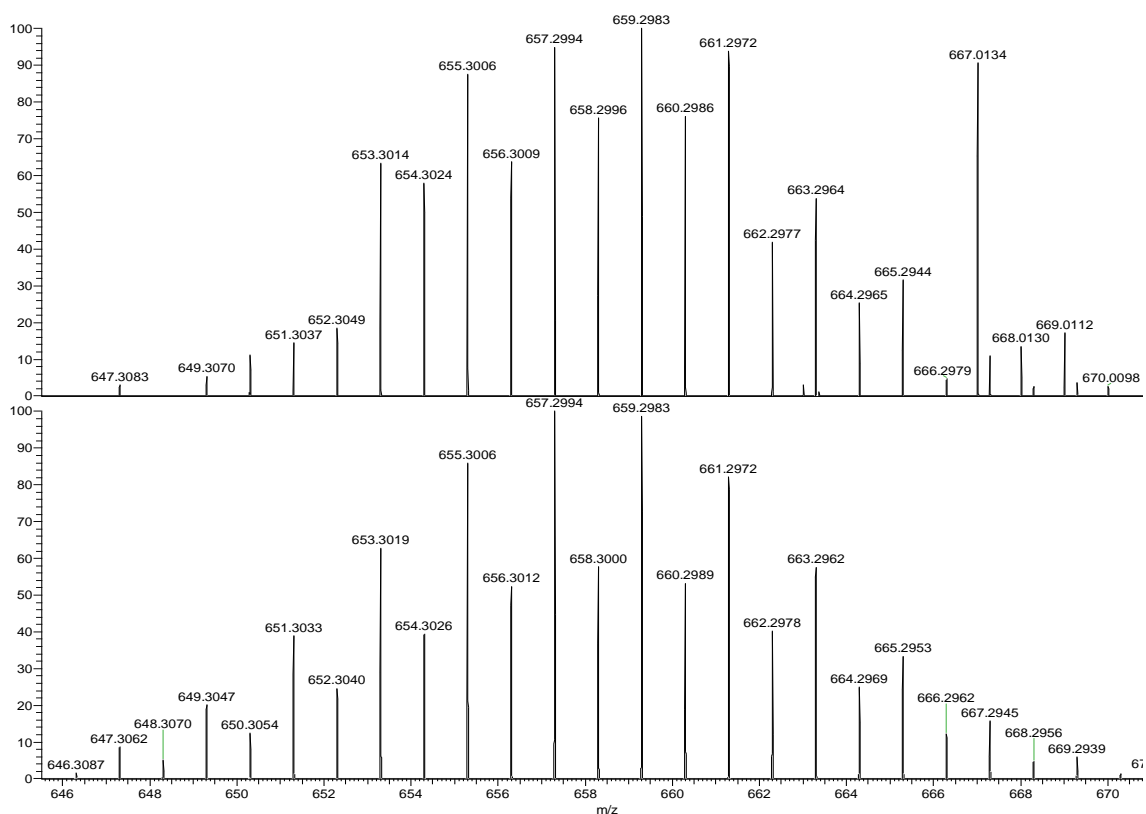


**Figure S13.** ESI(-) mass peak of  $(\text{Ge}_7\text{As}_2)^-$ . Measured (top) vs. calculated (bottom) spectrum.

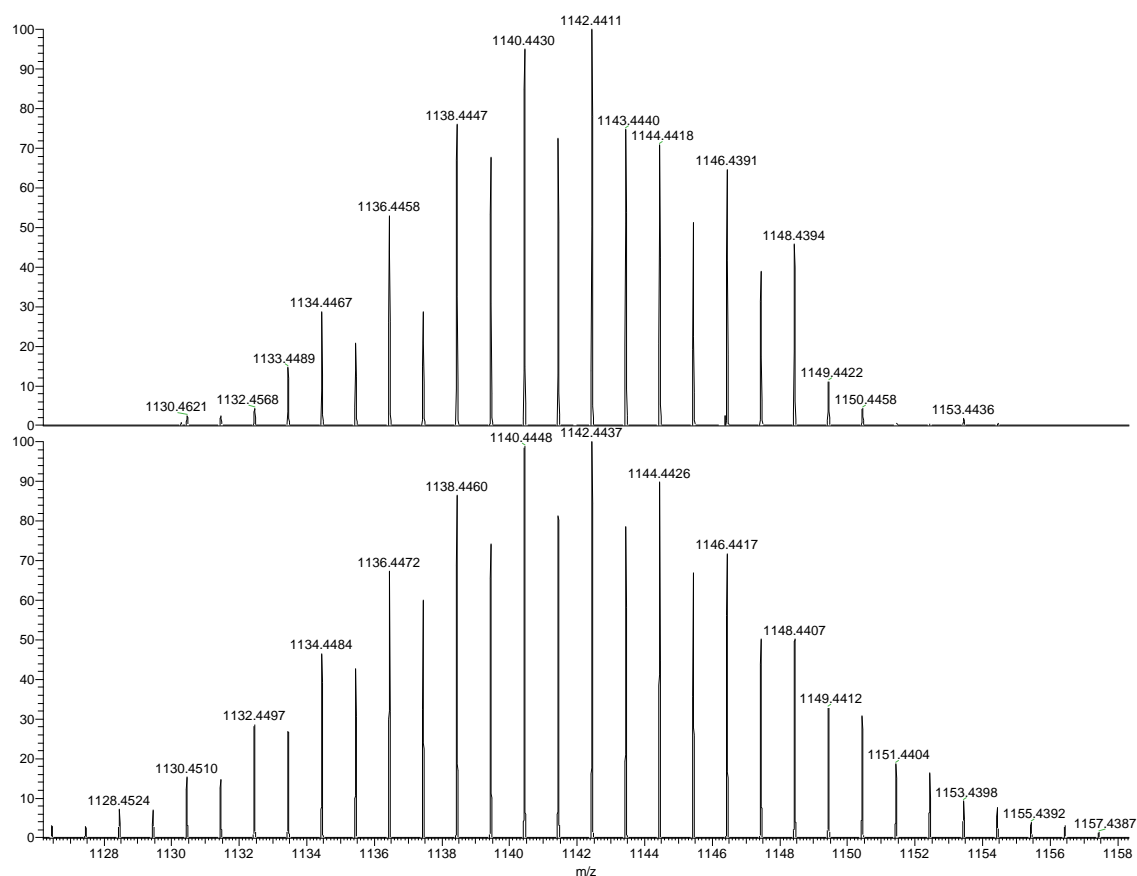


**Figure S14.** ESI(-) mass peak of  $(\text{Ge}_{10}\text{C}_{18}\text{H}_{36}\text{N}_2\text{O}_6\text{K})^-$ . Measured (top) vs. calculated (bottom) spectrum.

## 4.2 ESI-MS Investigation of $[K([2.2.2]crypt)]_3[Ge_8As_6Nb]$ (2)

The ESI(-)MS spectrum of **2** (Figure S15) revealed the cluster  $[Ge_8As_6Nb]^-$  ( $m/z = 1123.81$ ), which corresponds to the trimetallic cluster  $[Ge_8As_6Nb]^{3-}$  found in SCXD (Figure S16). Furthermore the mass peaks of  $(Ge_2As_2H)^-$  ( $m/z = 296.69$ ) was identified in the ESI(-) spectrum (Figure S17). Also mass peaks corresponding to a cluster with the composition  $[Ge_6As_6Nb]^-$  ( $m/z = 975.97$ ) and an overlay (mixture) of the following species were found:  $[Ge_7As_6NbH]^- / [Ge_7As_6Nb]^- / [Ge_6As_7NbH]^- / [Ge_6As_7Nb]^-$  ( $m/z = 1051.89$ ) (Figures S18, S19); the latter could, however, not be assigned unambiguously, and have not been confirmed yet by crystalline products. Nevertheless, these indicate further species to possibly co-exist in a complicated equilibrium in solution.

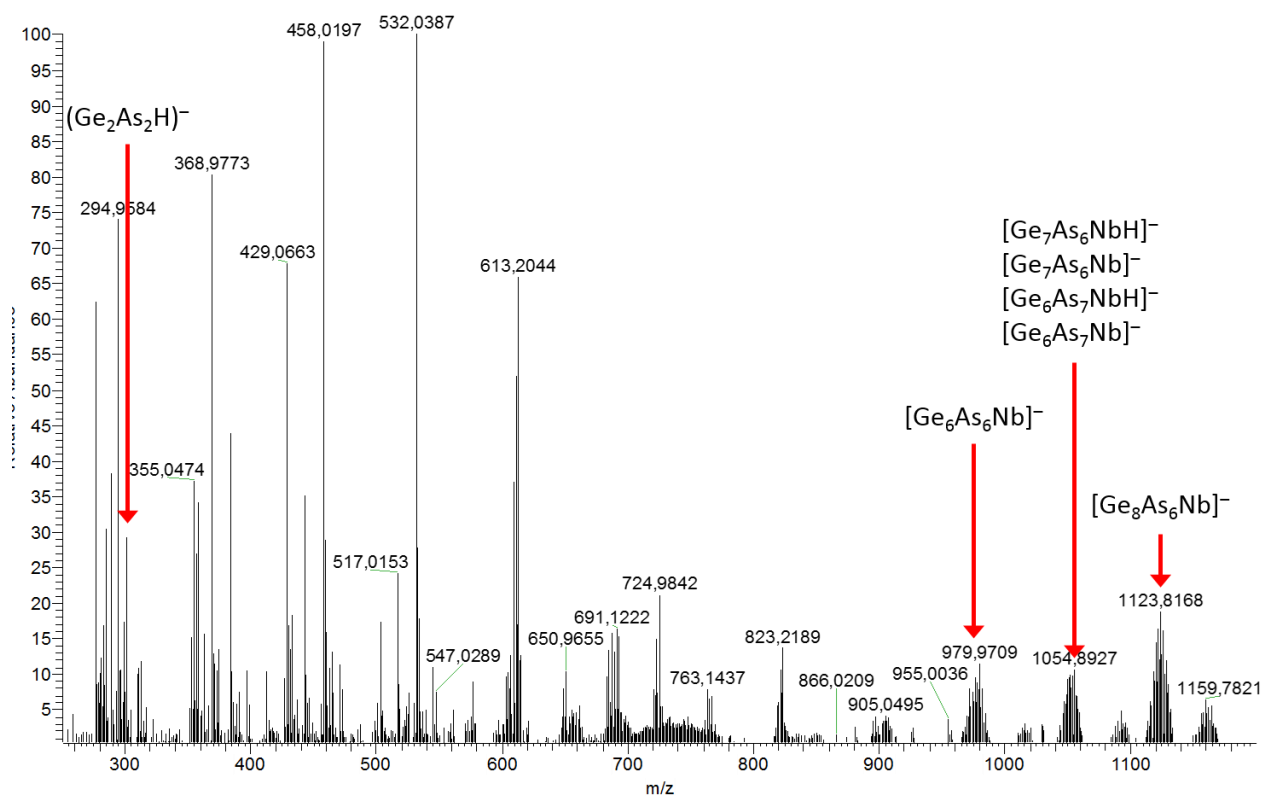


**Figure S15.** ESI-MS(-) overview spectrum



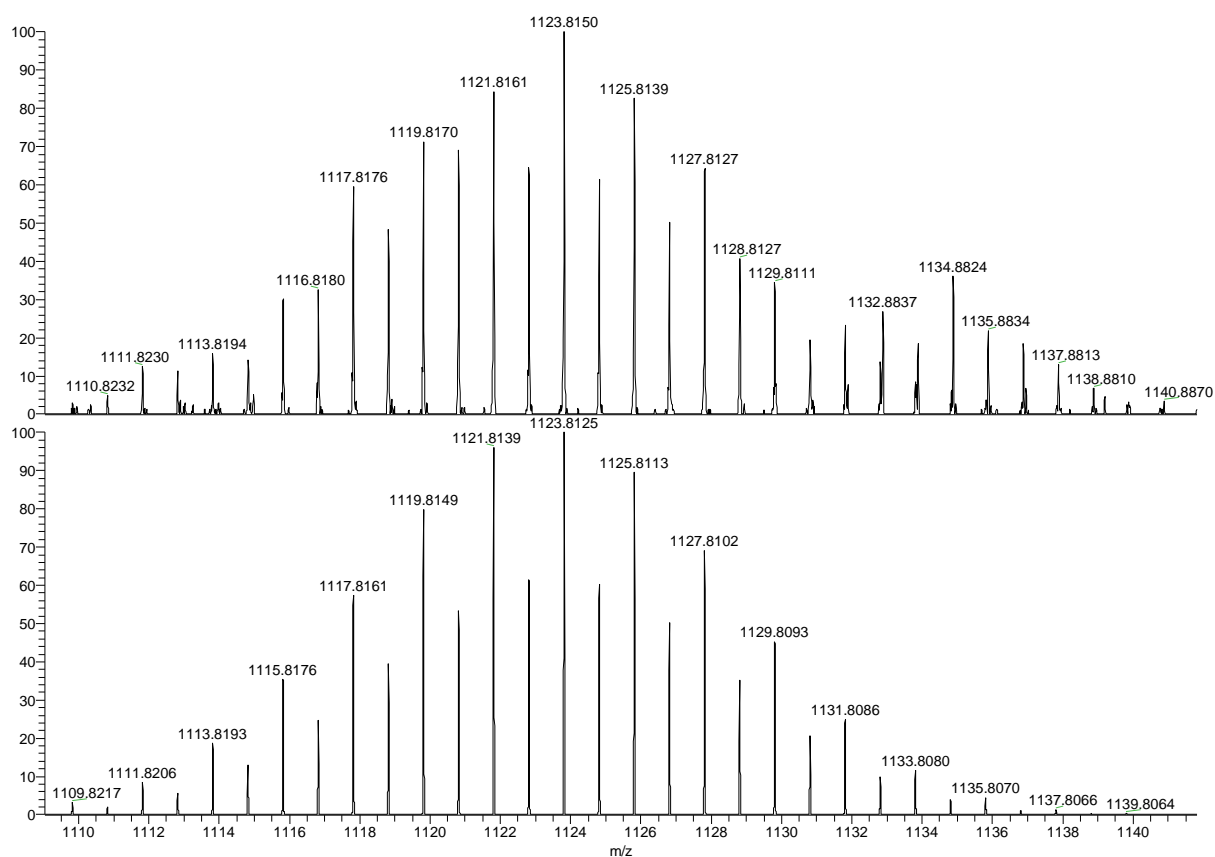


**Figure S16.** ESI(-) mass peak of  $[\text{Ge}_8\text{As}_6\text{Nb}]^-$ . Measured (top) vs. calculated (bottom) spectrum.

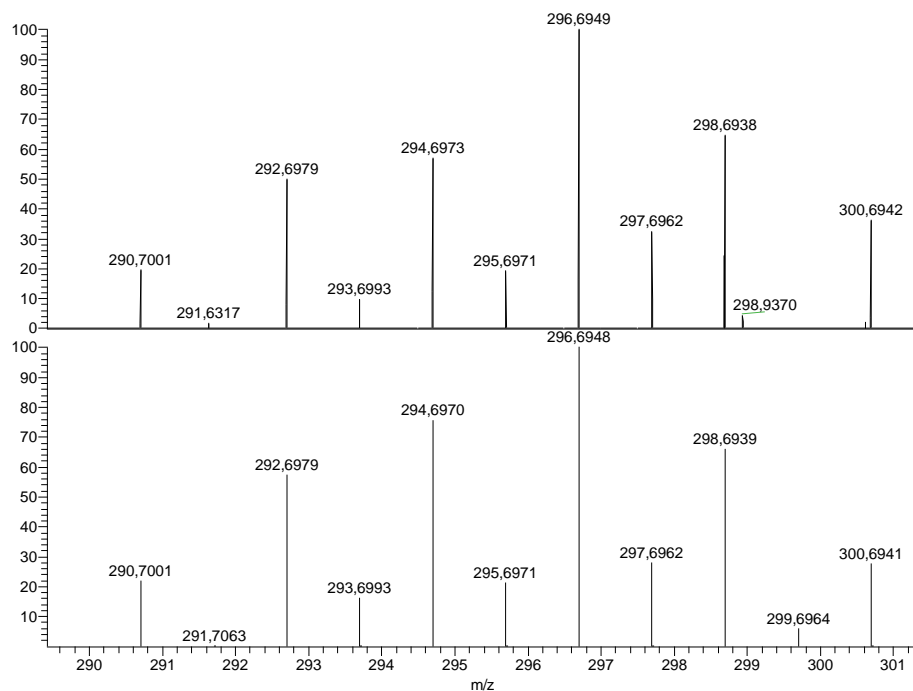


**Figure S17.** ESI(-) mass peak of  $(\text{Ge}_2\text{As}_2\text{H})^-$ . Measured (top) vs. calculated (bottom) spectrum.

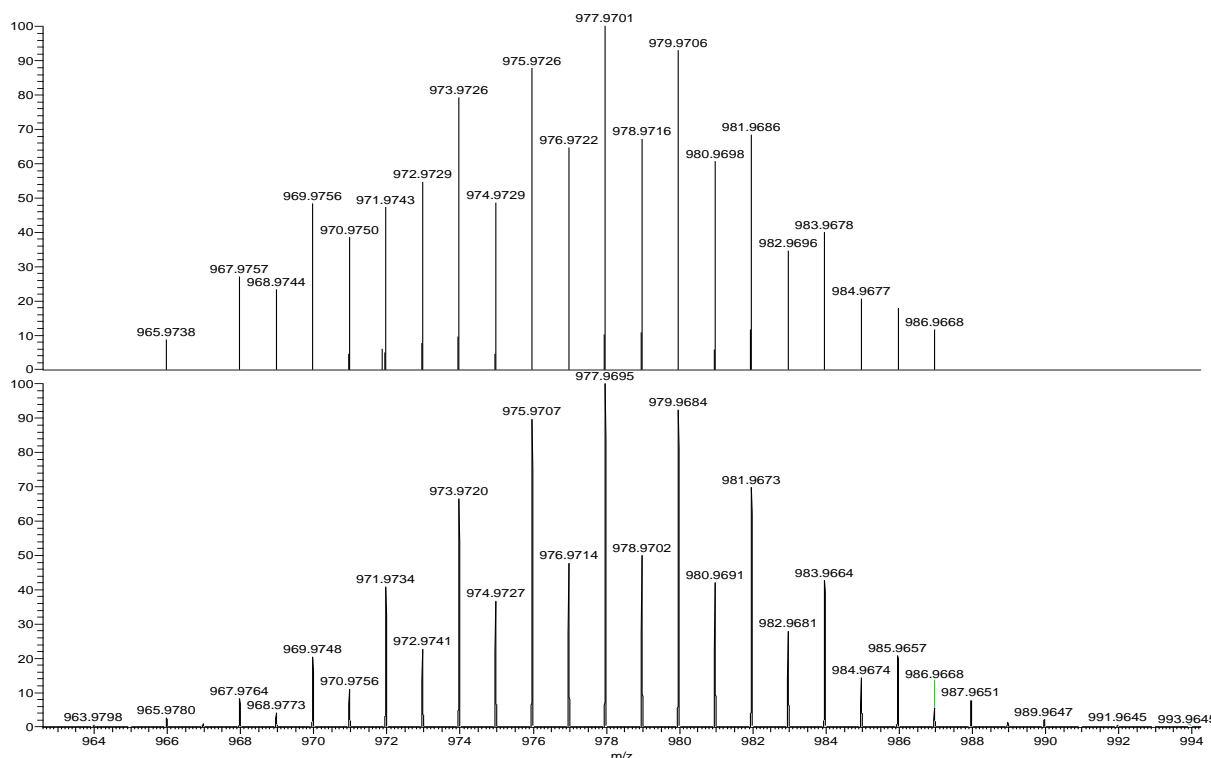


**Figure S18.** ESI(-) mass peak of  $[\text{Ge}_6\text{As}_6\text{Nb}]^-$ . Measured (top) vs. calculated (bottom) spectrum.

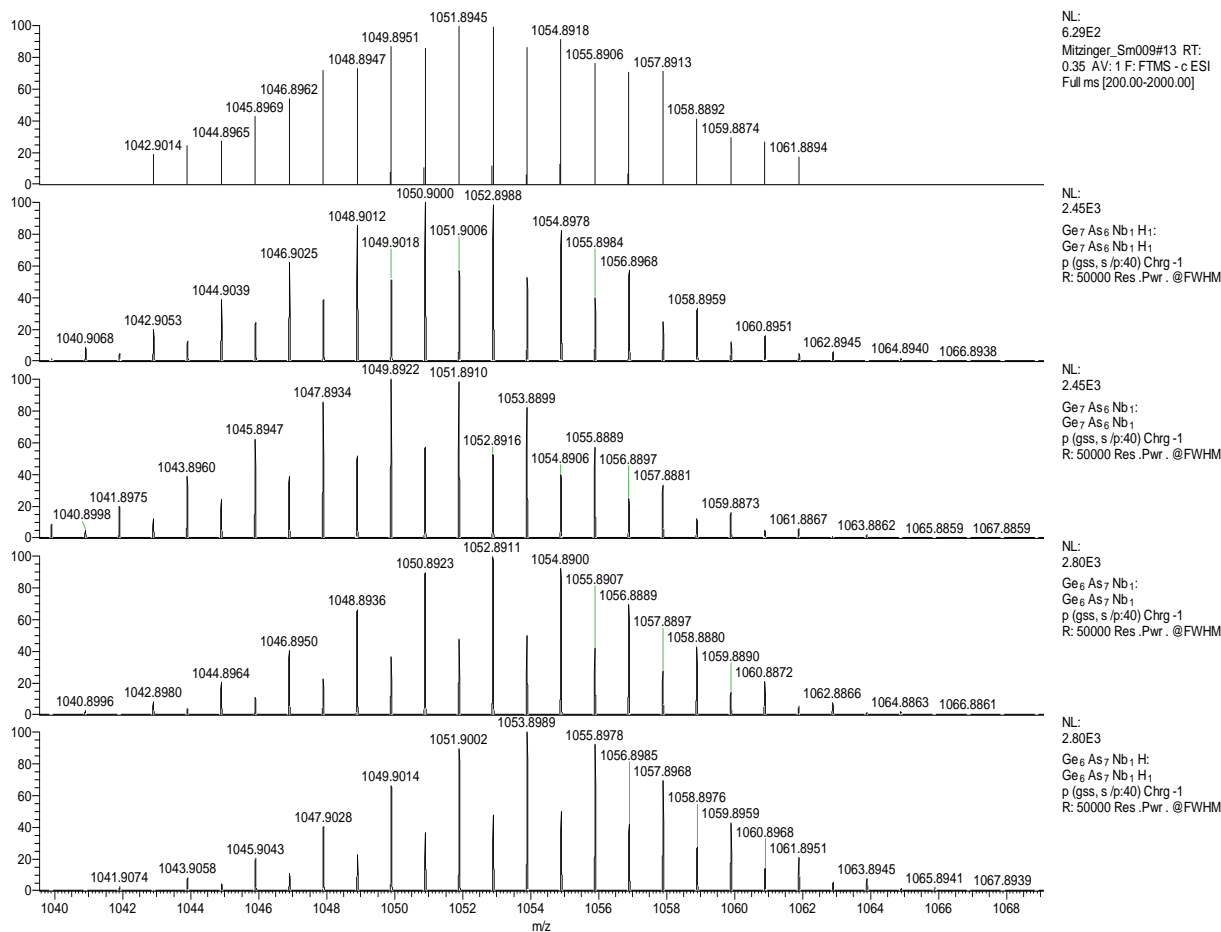


**Figure S19.** ESI(-) mass peak likely corresponding to  $[\text{Ge}_7\text{As}_6\text{Nb}]^- / [\text{Ge}_7\text{As}_6\text{NbH}]^- / [\text{Ge}_6\text{As}_7\text{Nb}]^- / [\text{Ge}_6\text{As}_7\text{NbH}]^-$ . Measured (top) vs. calculated (below) spectra.

## 5. Quantum Chemical Investigations

### 5.1 Methods

The DFT calculations were performed with the program system Turbomole.<sup>[3]</sup> The GGA exchange-correlation functional BP86 was applied,<sup>[4]</sup> together with a def-SVP basis set<sup>[5]</sup> and corresponding effective core potentials (ECPs) for Sn, Bi, Nb, and Rh.<sup>[6]</sup> COSMO was used with default parameters to compensate for the negative charge of the clusters.<sup>[7]</sup> The structures from Figure S20 and Tables S5 and S6 were drawn with the CYLview software.<sup>[8]</sup> Localization of MOs was done following the procedure by Boys.<sup>[9]</sup>

### 5.2 Perturbation theory study for atom assignment in the anions of 2

The optimal distribution of the different atom types (Ge/As) to the positions in the (trimetallic) cluster anions of compound **2** was done using first-order perturbation theory.<sup>[11,12]</sup> The (first-order) estimation for the preference of Ge and As to the different positions requires only the calculation of the electrostatic potential at the respective positions,  $V_i = V(\mathbf{R}_i)$ , without the contribution of the nucleus located at this position  $\mathbf{R}_i$ . As atoms (more right in the periodic table) are assigned to the sites with the lower electrostatic potential, Ge atoms are assigned to the remaining positions with a higher electrostatic potential. A detailed theoretical background of this method can be found in refs. 10 and 11.

For the anion of **1**,  $[\text{V@Ge}_8\text{As}_4]^{3-}$ , which is depicted in Figure S18, left hand side, many isomers exist that are very close in energy. Here the perturbation theory treatment leads to one of the structures that are lowest in energy according to explicit permutation of all possible atomic distributions, but not to the global minimum structure, which is by 2.0 kJ/mol lower in energy. However, as only slight changes in interatomic distances cause a change in the order of the isomer energies in this case, none of the results is more probable than the other. The result rather suggests a co-existence of several isomers – even in the crystal. For that, the isomer shown in Figure S20 (left) accords with the global minimum structure obtained by conservative permutation of the atoms.

For the anion of **2**,  $[\text{Nb@Ge}_8\text{As}_6]^{3-}$ , depicted in Figure S20 (right), the perturbation treatment afforded the global minimum structure that is separated from the next isomer in the order of increasing energy by 11 kJ/mol. During the perturbation theory treatment, the electrostatic potential was the highest at positions (2), (4)-(7), (11)-(13) and varies between  $-156.576$  and  $-156.565$  Hartree; the Ge atoms were placed here.

Positions (1), (3), (8)-(10), (14) have the lowest electrostatic potential ( $-160.927$  Hartree) and the six As atoms were assigned to these points.

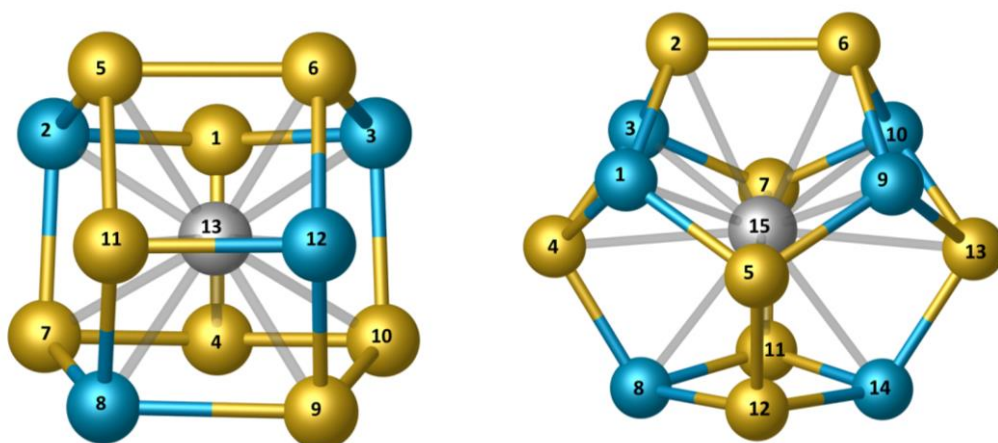
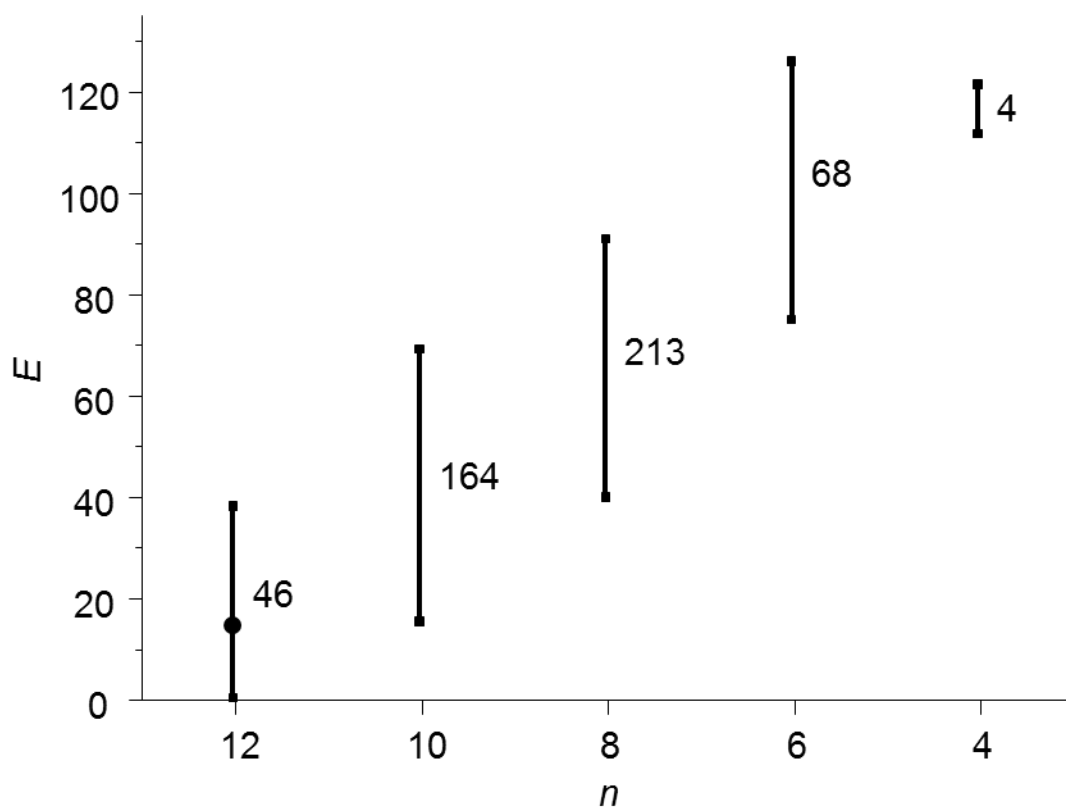


**Figure S20.** Left: Minimum structures of the  $[V@Ge_8As_4]^{3-}$  anion in **1** (left) and minimum structure of the  $[Nb@Ge_8As_6]^{3-}$  anion in **2** (right). Ge atoms are drawn in yellow and As atoms in blue.

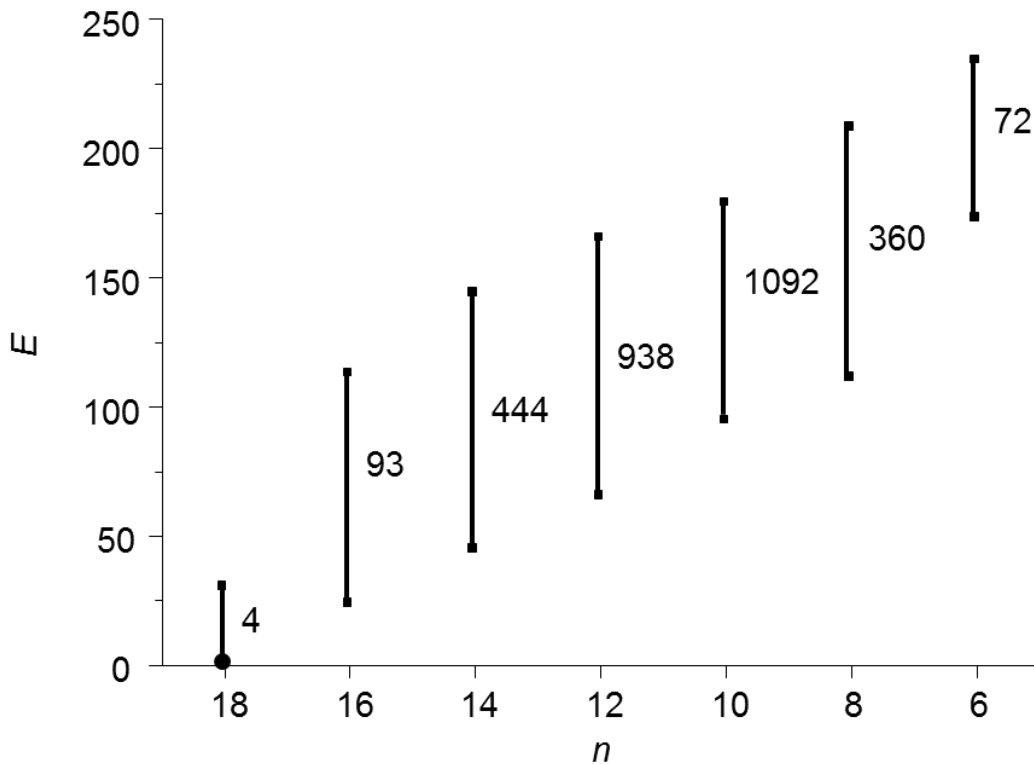
### 5.3 Isomers of the anions of **1** and **2**

We have calculated all isomers of the  $[V@Ge_8As_4]^{3-}$  and the  $[Nb@Ge_8As_6]^{3-}$  anion in **1** or **2**, respectively. According to many previous studies, the energetically lowest isomers are expected to be found among a series of isomers that possess the maximum number of heteroatomic bonds for each cluster type, i.e., 12 Ge–As bonds in  $[V@Ge_8As_4]^{3-}$  or 18 Ge–As bonds in  $[Nb@Ge_8As_6]^{3-}$ . The distributions obtained by perturbation theory are indeed the most favorable ones, but the others are close in energy. For comparison, all isomers were calculated based on the crystal structure geometry.

Figures S21 and S22 show the range of energies for all series of isomers of the anions  $[V@Ge_8As_4]^{3-}$  in **1** and  $[Nb@Ge_8As_6]^{3-}$  in **2**, respectively. For the 12-atom cage the least favorable isomer among the resulting non-equivalent 46 structures with 12 Ge–As bonds is higher in energy by 38.4 kJ/mol. For the 14-atom cage the second, third and fourth of the resulting non-equivalent isomers with 18 Ge–As bonds are higher in energy by 10.9, 20.3, or 29.7 kJ/mol, respectively. Tables S5 and S6 list structures and relative energies of the lowest-energy isomers of both cluster types.

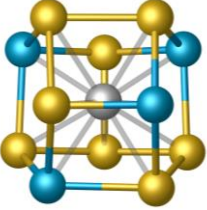
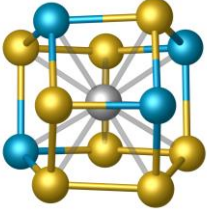
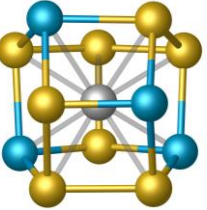
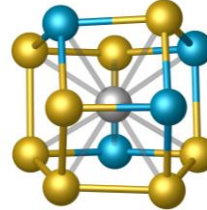
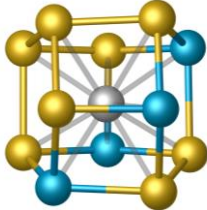
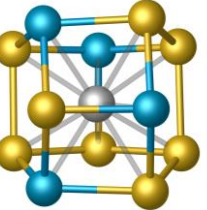
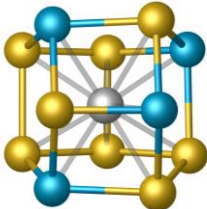
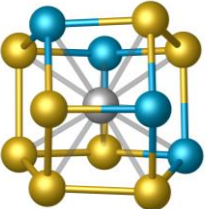
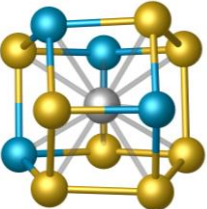


**Figure S21.** Numbers and energy ranges (in kJ/mol) calculated for series of isomers of the  $[V@Ge_8As_4]^{3-}$  anion in **1** that possess the same number  $n$  of (heteroatomic) Ge-As bonds.

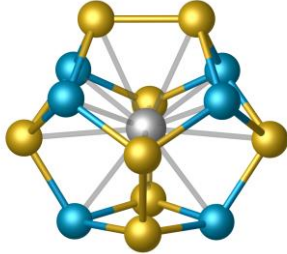
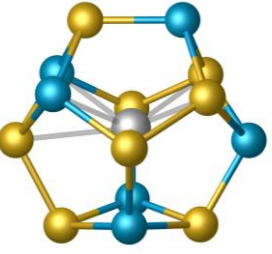
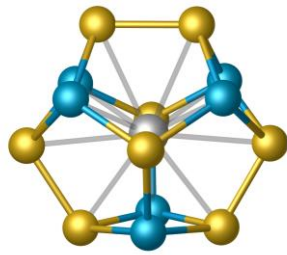
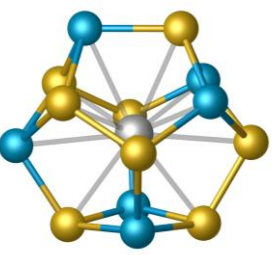


**Figure S22.** Numbers and energy ranges (in kJ/mol) calculated for series of isomers of the  $[Nb@Ge_8As_6]^{3-}$  anion in **2** that possess the same number  $n$  of (heteroatomic) Ge-As bonds.

**Table S5.** Structures and relative energies of the first nine calculated isomers (up to 5 kJ/mol) of  $[V@Ge_8As_4]^{3-}$  with a maximum number of heteroatomic bonds, i.e., 12 Ge–As bonds. Note that apparently identical clusters differ in structural details due to the missing molecular symmetry of the X-ray structure, which can cause different total energies.

Isomer structure	$\Delta E /$ kJ/mol	Isomer structure	$\Delta E /$ kJ/mol	Isomer structure	$\Delta E /$ kJ/mol
	0.0		2.0		3.2
	0.6		2.0		4.6
	1.5		3.2		4.6

**Table S6.** Structures and relative energies of the four calculated isomers of  $[Nb@Ge_8As_6]^{3-}$  with a maximum number of heteroatomic bonds, i.e., 18 Ge–As bonds. Note that apparently identical clusters differ in structural details due to the missing molecular symmetry of the X-ray structure, which can cause different total energies.

Isomer structure	$\Delta E /$ kJ/mol	Isomer structure	$\Delta E /$ kJ/mol
	0.0		20.3
	10.9		29.7

## 6. References for the supplementary information

- [1] (a) 4,7,13,16,21,24-Hexaoxa-1,10-diazabicyclo[8.8.8]hexacosane / Kryptofix 222; (b) B. Eisenmann, J. Klein, *J. Less Comm. Met.* 1991, **175**, 109; (c) H. G. von Schnering, J. Wolf, D. Weber, R. Ramirez and T. Meyer, *Angew. Chem. Int. Ed.*, 1986, **25**, 353.
- [2] (a) X'Pert Highscore Plus, Version 2.2c, Panalytical B.V., Almelo, The Netherlands, 2007; (b) G. M. Sheldrick, *Acta Crystallogr.* **2008**, **A64**, 112.
- [3] TURBOMOLE Version 6.6, © TURBOMOLE GmbH 2014. TURBOMOLE is a development of University of Karlsruhe and Forschungszentrum Karlsruhe 1989 – 2007, TURBOMOLE GmbH since 2007; available from <http://www.turbomole.com>.
- [4] (a) D. Becke, *Phys. Rev. A* 1988, **38**, 3098; (b) J. P. Perdew, *Phys. Rev. B* 1996, **33**, 8822.
- [5] (a) K. Eichkorn, F. Weigend, O. Treutler and R. Ahlrichs, *Theor. Chem. Acc.*, 1997, **97**, 119; (b) K. Eichkorn, O. Treutler, H. Öhm, M. Häser and R. Ahlrichs, *Chem. Phys. Lett.*, 1995, **242**, 652.
- [6] (a) M. Dolg, H. Stoll, A. Savin and H. Preuss, *Theor. Chim. Acta* 1989, **75**, 173; (b) H. Stoll, B. Metz and M. Dolg, *J. Comput. Chem.* 2002, **23**, 767.
- [7] (a) A. Klamt and G. Schürmann, *J. Chem. Soc. Perkin Trans.* 1993, **2**, 799; (b) A. Schäfer, A. Klamt, D. Sattel, J. C. W. Lohrenz and F. Eckert, *Phys. Chem. Chem. Phys.*, 2000, **2**, 2187.
- [8] CYLview, v1.0b; C. Y. Legault, Université de Sherbrooke, 2009.  
<http://www.cylview.org>
- [9] (a) S. F. Boys, *Rev. Mod. Phys.* 1960, **32**, 296; (b) J. M. Foster and S. F. Boys, *Rev. Mod. Phys.* 1960, **32**, 300.
- [10] (a) F. Weigend, C. Schrodtr and R. Ahlrichs, *J. Chem. Phys.* 2004, **121**, 10380; (b) F. Weigend and C. Schrodtr, *Chem. Eur. J.* 2005, **11**, 3559.
- [11] F. Weigend, *J. Chem. Phys.* 2014, **141**, 134103.